A R C H I V E S O F M E T A L L U R G Y A N D M A T E R I A L S
Volume 57 2012 Issue 4
DOI: 10.2478/v10172-012-0133-1

T. SKRZYPCZAK*

SHARP INTERFACE NUMERICAL MODELING OF SOLIDIFICATION PROCESS OF PURE METAL

SPOSÓB MODELOWANIA NUMERYCZNEGO PROCESU KRZEPNIĘCIA Z OSTRYM FRONTEM

The paper is focused on the study of the solidification process of pure metals, in which the solidification front is smooth. It has the shape of a surface separating liquid from solid in three dimensional space or a curve in 2D. The location and topology of moving interface change over time and its velocity depends on the values of heat fluxes on the solid and liquid side of it.

Such a formulation belongs to a group called Stefan problems. A mathematical model of the Stefan problem is based on differential equations of heat conduction and interface motion. This system of equations is supplemented by appropriate initial and boundary conditions as well as the continuity conditions at the solidification interface. The solution involves the determination of temporary temperature field and interface position. Typically, it is impossible to obtain the exact solution of such problem.

This paper presents a mathematical model for the two-dimensional problem. The equation of heat conduction is supplemented with Dirichlet and Neumann boundary conditions. Interface motion is described by the level set equation which solution is sought in the form of temporary distribution of the signed distance function. Zero level of the distance field coincides with the position of the front. Values of the signed distance function obtained from the level set equation require systematic reinitialization.

Numerical model of the process based on the finite element method (FEM) is also presented. FEM equations are derived and discussed. The explicit time integration scheme is proposed. It helps to avoid solving the system of equations during each time step. The reinitialization procedure of the signed distance function is described in detail. Examples of numerical analysis of the solidification process of pure copper within the complex geometry are presented. Results obtained from the use of constant material properties are compared with those obtained from the use of temperature dependent properties.

Keywords: Pure Metal, Stefan Problem, Sharp Interface, Solidification, Finite Element Method, Level Set Method

W pracy skupiono się na badaniu procesu krzepnięcia czystych metali, podczas którego front krzepnięcia pozostaje płaski. W przypadku trójwymiarowym jest on powierzchnią oddzielającą ciecz od ciała stałego, w przypadku dwuwymiarowym ma postać krzywej. Położenie i topologia frontu krzepnięcia zmienia się w czasie, a prędkość przemieszczania zależy od różnicy wartości strumieni cieplnych po stronie ciała stałego i cieczy.

Takie sformułowanie klasyfikuje opisywane zjawisko w grupie tzw. zagadnień Stefana. Model matematyczny tego procesu stanowią równania różniczkowe przewodnictwa ciepła oraz ruchu powierzchni międzyfazowej. Układ ten uzupełniają odpowiednie warunki brzegowe, początkowe oraz warunki ciągłości na froncie. Jego rozwiązanie polega na wyznaczeniu chwilowych pól temperatury oraz położenia frontu. Najczęściej nie da się uzyskać rozwiązania tak sformułowanego problemu w sposób dokładny.

W pracy zaprezentowano model matematyczny zagadnienia dla przypadku płaskiego. Równanie różniczkowe przewodnictwa ciepła uzupełniono warunkami brzegowymi Dirichleta oraz Neumanna. Ruch interfejsu międzyfazowego opisano tzw. równaniem poziomic (ang. level set equation), którego rozwiązania poszukiwano w postaci chwilowego rozkładu funkcji dystansu. Izolinia zerowa tego rozkładu pokrywa się z położeniem frontu. Otrzymane wartości funkcji dystansu wymagają systematycznej reinicjalizacji.

Przedstawiono również model numeryczny procesu bazujący na metodzie elementów skończonych. Opisano schemat postępowania prowadzący do otrzymania dyskretnych równań MES. Wykorzystano jawny schemat całkowania po czasie, co pozwoliło uniknąć konieczności rozwiązywania układu równań zarówno w przypadku równania przewodnictwa ciepła jak i równania poziomic. Szczegółowo opisano metodę reinicjalizowania funkcji dystansu. Zaprezentowano przykłady analizy numerycznej procesu krzepnięcia czystej miedzi w obszarze o złożonej geometrii. Porównano wyniki otrzymane dla stałych własności materiałowych z wynikami uzyskanymi z wykorzystaniem własności zależnych od temperatury.

* INSTITUTE OF MECHANICS AND MACHINE DESIGN, CZESTOCHOWA UNIVERSITY OF TECHNOLOGY, 42-201 CZĘSTOCHOWA, 73 DABROWSKIEGO STR., POLAND

1. Introduction

Sharp interface solidification belongs to a large set of so called phase transition problems. They are thermodynamic processes in which material changes its physical state. These processes occur due to temperature, pressure, etc., and a transition from one state to another is often discontinuous. Examples of such processes include, for example freezing of water, evaporation, melting and solidification of metals and alloys, etc. Solidification of a pure metal belongs to the group of Stefan problems which describe various phenomena that take place with the existence of a sharp internal interface. In 1831, Lame and Clapeyron dealt with such problems for the first time. The name ”Stefan problems” comes from the name of the Austrian scientist Joseph Stefan, who worked in 1890 on determining the speed of the front of freezing water.

Solidification process considered on a macroscopic scale can be done in two ways. In the case of alloy solidification front usually loses stability. This phenomenon is caused by segregation of the components on the front and called solutal undercooling [1-4]. It leads to the destabilization of the shape of the front and the formation of a mushy zone. Even when the explicit effect of macrosegregation is neglected one can consider it indirectly adopting one of the models based on the solidification between the solidus and liquidus temperatures [5-10].

During solidification of pure metal interface stabilty depends on the direction of heat flow [2]. In the case of directional solidification temperature of the liquid T^l always increases ahead of the interface, therefore the heat flow direction is opposite that of solid phase growth. When a perturbation of amplitude Δx appears at an smooth interface, the heat flow through its tip increases (Fig. 1). Therefore, temperature $T_1^l < T_2^l$ and more heat is transported from the liquid to the tip of the perturbation rather than a recess. As a result, the perturbation melts back and the planar interface is stabilized. In equiaxed solidification, the opposite process takes place.

Interface tracking methods are generally based on the phase-field method, level set method (LSM) or cellular automata [11]. The basic idea of the phase-field method is to introduce a phase-field variable that varies smoothly from zero to unity between the solid and liquid phases over the region, which has a small but numerically resolvable thickness [12-14]. LSM is an alternative method to track the sharp interface directly. It is widely used in various applications such as two-phase flow, crack propagation, computer vision and image processing. In this method, interfacial geometric quantities such as curvature and outward normal can be easily calculated using the level set variable φ. The method was first applied to Stefan problems in [15].

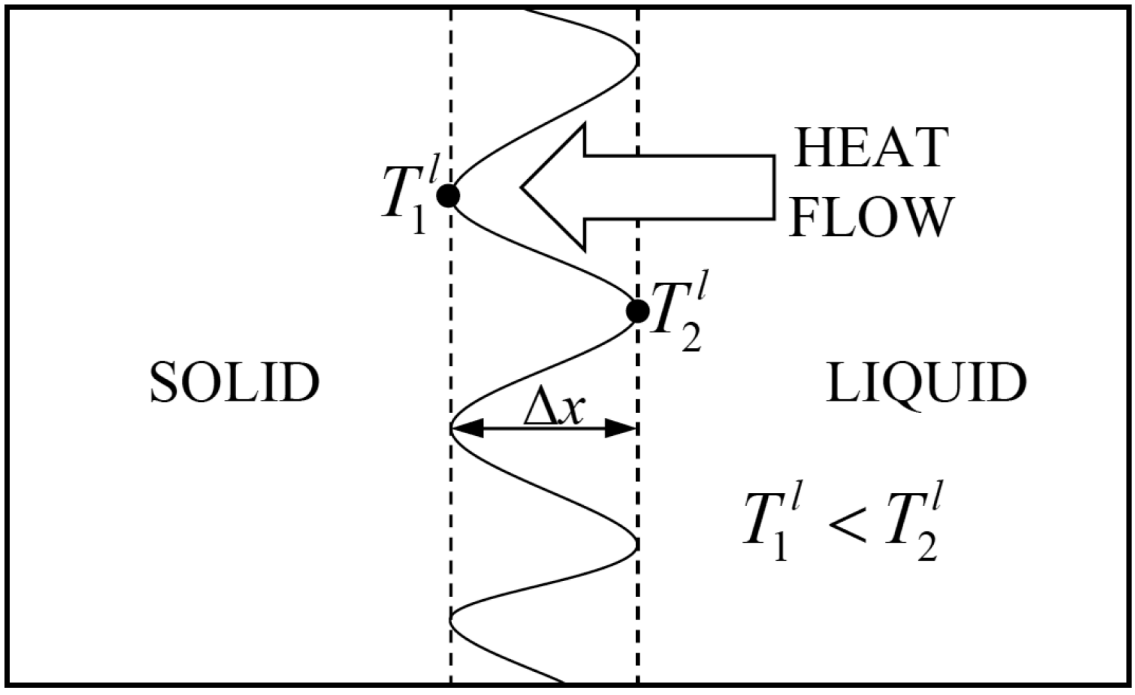

Fig. 1. Perturbations on a flat front during directional solidification of pure metal

Computer simulations of the solidification process with a sharp front, such as pure metal solidification process is a challenge for developers of specialized software. When building solver one have to consider the possibility of interfaces of any shape. Another important requirement of the software is the correct calculation of the temperature distribution on both sides of the front. It is known, that the temporary position of the front can be any. This means that it can be arbitrarily positioned between the nodes, which leads to considerable difficulties in determining the temperature along it.

Stefan problem for solidification or melting processes, which are described in the literature can be divided into three groups:

- methods based on modifications of approximation functions in finite elements cut by the solidification interface. In this approach the finite element mesh does not change with time [16];
- methods based on the adaptation of mesh. In this case, the edges of the finite elements are matched to the shape of the front [17];
- method based on the fuzzy front. Solidification at a constant temperature is replaced by a process which takes place in a narrow temperature range, as in the case of alloys [18, 19].

2. Mathematical model of solidification

Process of directional solidification of pure metal in the two-dimensional area is considered. Natural convection of the liquid phase is omitted in the model. Process scheme is shown in Fig. 2. Region containing liquid phase Ω_L is separated from the solidified one Ω_S. Separation curve is sharp moving interface Γ_{LS}, which runs between them.

During directional solidification, heat is transported in the direction of the solid, which results in growth of the solid phase. The rate of growth of the solid has a direct influence on the position of Γ_{LS}.

Governing equations of the mathematical model are as follows

Transient heat conduction equation:

$$\frac{\partial}{\partial x}\left(\lambda\frac{\partial T}{\partial x}\right)+\frac{\partial}{\partial y}\left(\lambda\frac{\partial T}{\partial y}\right)-c\rho\frac{\partial T}{\partial t}=0 \tag{1}$$

where $T = T(x,y,t)$ is the temperature [K], $\lambda = \lambda(T)$ – coefficient of thermal conductivity [J s^{-1} m^{-1} K^{-1}], $c = c(T)$ – specific heat [J kg^{-1} K^{-1}], $\rho = \rho(T)$ – density [kg m^{-3}], t – time [s], x, y - Cartesian coordinates [m].

Level set equation that governs the movement of Γ_{LS}:

$$u_x\frac{\partial\phi}{\partial x}+u_y\frac{\partial\phi}{\partial y}+\frac{\partial\phi}{\partial t}=0 \tag{2}$$

where $\varphi = \varphi(x,y,t)$ is a signed distance function that measures the distance between a particular point and solidification interface [m], u_x, u_y – components of the interface velocity vector [m s^{-1}].

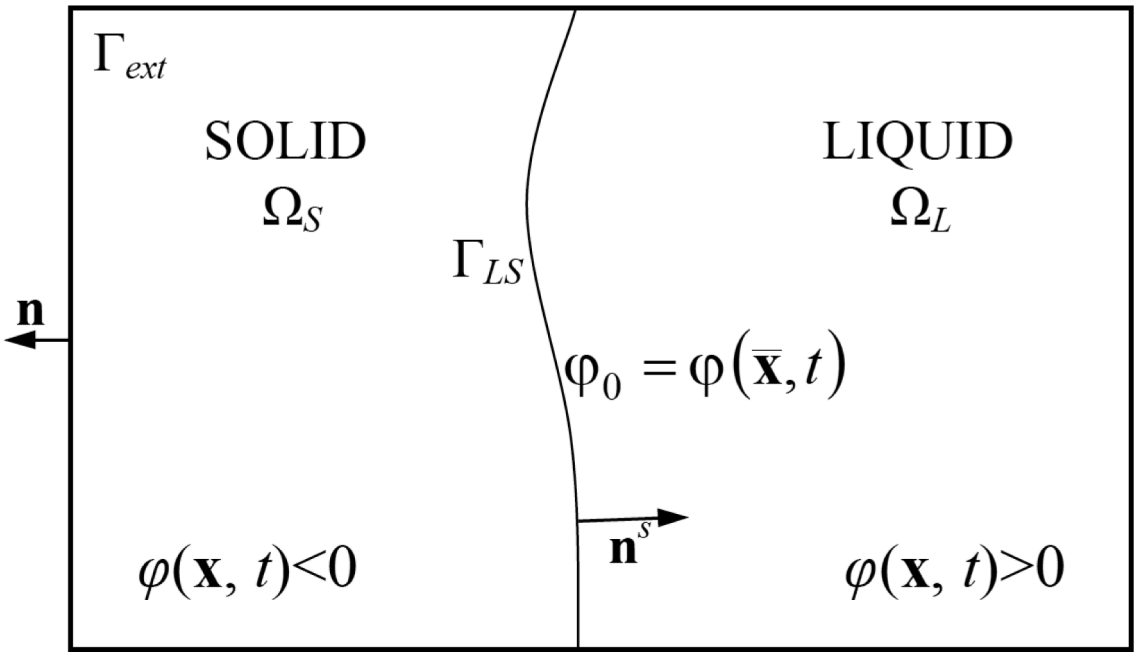

Fig. 2. Directional solidification scheme of pure metal

φ is a function of position and time, which meets the following conditions resulting from the LSM [20-22]:

$$\varphi(\mathbf{x},t) = \min_{\bar{x}\in\Gamma_{LS}} \|\mathbf{x}-\bar{\mathbf{x}}\| \operatorname{sgn}\left(\mathbf{n}^s \cdot (\mathbf{x}-\bar{\mathbf{x}})\right) \tag{3}$$

where $\mathbf{n}^s$ is the normal vector pointing outwards Γ_{LS}, $\bar{\mathbf{x}}$ is a vector of the position of Γ_{LS}.

Distance function φ can take the following values

$$\begin{aligned} &\phi(\mathbf{x},t) > 0,\ \mathbf{x} \in \Omega_L \\ &\phi(\mathbf{x},t) = 0,\ \mathbf{x} \in \Gamma_{LS} \\ &\phi(\mathbf{x},t) < 0,\ \mathbf{x} \in \Omega_S \end{aligned} \tag{4}$$

The mathematical model is supplemented with appropriate initial and boundary conditions as well as the continuity conditions at the interface.

The initial conditions:

$$T|_{t=0} = T_0 \tag{5}$$

$$\phi|_{t=0} = \phi_0 \tag{6}$$

The boundary conditions:

$$T|_{\Gamma_{ext}} = T_b \tag{7}$$

$$-\lambda \frac{\partial T}{\partial n}\bigg|_{\Gamma_{ext}} = q \tag{8}$$

The continuity conditions at Γ_{LS}:

$$T^s|_{\Gamma_{LS}} = T^l\big|_{\Gamma_{LS}} = T_M \tag{9}$$

$$\lambda_s \frac{\partial T^s}{\partial n^s}\bigg|_{\Gamma_{LS}} - \lambda_l \frac{\partial T^l}{\partial n^s}\bigg|_{\Gamma_{LS}} = \rho_s L |\mathbf{u}| \tag{10}$$

where $T_0 = T_0(x,y)$ is the initial temperature [K], $\varphi_0 = \varphi_0(x,y)$ – the initial position of solidification front [m], $T_b = T_b(x,y)$ – a given boundary temperature [K], Γ_{ext} – the external boundary, n – the direction of the vector pointing outwards Γ_{ext}, n^s – the direction of the vector pointing outwards Γ_{LS}, T_M – melting (solidification) temperature [K], q – heat flux normal to the external boundary Γ_{ext} [J s^{-1} m^{-2}], $\mathbf{u}$ – velocity of the solidification front, L – latent heat of solidification [J kg^{-1}], s, l – means a solid or liquid.

3. Finite element formulation

In accordance with the weighted residuals method, equations (1-2) are multiplied by a weight function $w = w(x,y)$ then integrated over the region $\Omega = \Omega_S \cup \Omega_L$.

$$\iint_\Omega w\left[\frac{\partial}{\partial x}\left(\lambda\frac{\partial T}{\partial x}\right) + \frac{\partial}{\partial y}\left(\lambda\frac{\partial T}{\partial y}\right) - c\rho\frac{\partial T}{\partial t}\right]dxdy = 0 \tag{11}$$

$$\iint_\Omega w\left[u_x\frac{\partial \phi}{\partial x} + u_y\frac{\partial \phi}{\partial y} + \frac{\partial \phi}{\partial t}\right]dxdy = 0 \tag{12}$$

In order to reduce the order of the equation (11) Green's theorem is used, which leads to the following weak form

$$\begin{aligned} &\iint_\Omega \lambda\left(\frac{\partial w}{\partial x}\frac{\partial T}{\partial x} + \frac{\partial w}{\partial y}\frac{\partial T}{\partial y}\right)dxdy \\ &+ \iint_\Omega c\rho w\frac{\partial T}{\partial t}dxdy = \oint_{\Gamma_{ext}} \lambda w\frac{\partial T}{\partial n}ds \end{aligned} \tag{13}$$

FEM equations are derived according to the Galerkin method, where the weight functions $w(x,y)$ are the same as the shape functions $N(x,y)$. The whole region is spatially discretized with the use of a triangular mesh. Temperature T, the distance φ and their spatial and time derivatives are approximated as follows

$$T(x,y,t) = \sum_{i=1}^{3} N_i(x,y)\,T_i = [N]\{T\} \tag{14}$$

$$\begin{aligned} \frac{\partial T(x,y,t)}{\partial x} &= \sum_{i=1}^{3}\frac{\partial N_i(x,y)}{\partial x}T_i = [D_x]\{T\}, \\ \frac{\partial T(x,y,t)}{\partial y} &= \sum_{i=1}^{3}\frac{\partial N_i(x,y)}{\partial y}T_i = \left[D_y\right]\{T\} \end{aligned} \tag{15}$$

$$\frac{\partial T(x,y,t)}{\partial t} = \sum_{i=1}^{3} N_i(x,y)\frac{\partial T_i}{\partial t} = [N]\left\{\frac{\partial T}{\partial t}\right\} \tag{16}$$

$$\lambda\frac{\partial T}{\partial n} = -\sum_{i=1}^{2}\tilde{N}_i(\xi)\,q_i = \left[\tilde{N}\right]\{q\} \tag{17}$$

$$\phi(x,y,t) = \sum_{i=1}^{3} N_i(x,y)\,\phi_i = [N]\{\phi\} \tag{18}$$

$$\begin{aligned} \frac{\partial \phi(x,y,t)}{\partial x} &= \sum_{i=1}^{3}\frac{\partial N_i(x,y)}{\partial x}\phi_i = [D_x]\{\phi\}, \\ \frac{\partial \phi(x,y,t)}{\partial y} &= \sum_{i=1}^{3}\frac{\partial N_i(x,y)}{\partial y}\phi_i = \left[D_y\right]\{\phi\} \end{aligned} \tag{19}$$

$$\frac{\partial \phi(x,y,t)}{\partial t} = \sum_{i=1}^{3} N_i(x,y)\frac{\partial \phi_i}{\partial t} = [N]\left\{\frac{\partial \phi}{\partial t}\right\} \tag{20}$$

where ξ is the coordinate measured along the external edge $\Gamma_{ext}^{(e)}$ of the triangular element, $\left[\tilde{N}\right] = \begin{bmatrix} \tilde{N}_1 & \tilde{N}_2 \end{bmatrix}$ are the shape functions at $\Gamma_{ext}^{(e)}$ and the remaining vectors are defined as follows

$$\begin{aligned} [N] &= \begin{bmatrix} N_1 & N_2 & N_3 \end{bmatrix}, \quad [D_x] = \begin{bmatrix} \frac{\partial N_1}{\partial x} & \frac{\partial N_2}{\partial x} & \frac{\partial N_3}{\partial x} \end{bmatrix}, \\ \left[D_y\right] &= \begin{bmatrix} \frac{\partial N_1}{\partial y} & \frac{\partial N_2}{\partial y} & \frac{\partial N_3}{\partial y} \end{bmatrix} \end{aligned} \tag{21}$$

$$\{T\} = \begin{Bmatrix} T_1 \\ T_2 \\ T_3 \end{Bmatrix}, \quad \left\{\frac{\partial T}{\partial t}\right\} = \begin{Bmatrix} \partial T_1/\partial t \\ \partial T_2/\partial t \\ \partial T_3/\partial t \end{Bmatrix}, \quad \{q\} = \begin{Bmatrix} q_1 \\ q_2 \end{Bmatrix} \tag{22}$$

$$\{\phi\} = \begin{Bmatrix} \phi_1 \\ \phi_2 \\ \phi_3 \end{Bmatrix}, \quad \left\{\frac{\partial \phi}{\partial t}\right\} = \begin{Bmatrix} \partial \phi_1/\partial t \\ \partial \phi_2/\partial t \\ \partial \phi_3/\partial t \end{Bmatrix} \tag{23}$$

Relations (14-20) are inserted into (12-13) leading to the following equations for a single finite element

$$\lambda^{(e)} \iint_{\Omega^{(e)}} \left([D_x]^T [D_x] + \left[D_y\right]^T \left[D_y\right] \right) dxdy \{T\} + (c\rho)^{(e)} \iint_{\Omega^{(e)}} [N]^T [N] \, dxdy \left\{\frac{\partial T}{\partial t}\right\} = - \oint_{\Gamma_{ext}^{(e)}} \left[\tilde{N}\right]^T \left[\tilde{N}\right] ds \{q\} \tag{24}$$

$$\iint_{\Omega^{(e)}} \left(u_x^{(e)} [N]^T [D_x] + u_y^{(e)} [N]^T \left[D_y\right] \right) dxdy \{\phi\} + \iint_{\Omega^{(e)}} [N]^T [N] \, dxdy \left\{\frac{\partial \phi}{\partial t}\right\} = 0 \tag{25}$$

Above equations contain matrices (or vectors) that can be written as

$$\mathbf{K}_T^{(e)} = \lambda^{(e)} \iint_{\Omega^{(e)}} \left([D_x]^T [D_x] + \left[D_y\right]^T \left[D_y\right] \right) dxdy \tag{26}$$

$$\mathbf{M}_T^{(e)} = (c\rho)^{(e)} \iint_{\Omega^{(e)}} [N]^T [N] \, dxdy \tag{27}$$

$$\mathbf{B}_T^{(e)} = - \oint_{\Gamma_{ext}^{(e)}} \left[\tilde{N}\right]^T \left[\tilde{N}\right] ds \{q\} \tag{28}$$

$$\mathbf{A}_\phi^{(e)} = \iint_{\Omega^{(e)}} \left(u_x^{(e)} [N]^T [D_x] + u_y^{(e)} [N]^T \left[D_y\right] \right) dxdy \tag{29}$$

$$\mathbf{M}_\phi^{(e)} = \iint_{\Omega^{(e)}} [N]^T [N] \, dxdy \tag{30}$$

$$\mathbf{T}^{(e)} = \{T\}, \quad \dot{\mathbf{T}}^{(e)} = \left\{\frac{\partial T}{\partial t}\right\}, \quad \boldsymbol{\varphi}^{(e)} = \{\phi\}, \quad \dot{\boldsymbol{\varphi}}^{(e)} = \left\{\frac{\partial \phi}{\partial t}\right\} \tag{31}$$

where $\mathbf{K}_T^{(e)}$ is the thermal conductivity matrix, $\mathbf{M}_T^{(e)}$ – heat capacity matrix, $\mathbf{B}_T^{(e)}$ – vector associated with the boundary conditions, $\mathbf{A}_\phi^{(e)}$ – advection matrix, $\mathbf{M}_\phi^{(e)}$ – mass matrix.

Substituting (26-31) into (24-25) leads to the matrix form of the local FEM equations

$$\mathbf{K}_T^{(e)} \mathbf{T}^{(e)} + \mathbf{M}_T^{(e)} \dot{\mathbf{T}}^{(e)} = \mathbf{B}_T^{(e)} \tag{32}$$

$$\mathbf{A}_\phi^{(e)} \boldsymbol{\varphi}^{(e)} + \mathbf{M}_\phi^{(e)} \dot{\boldsymbol{\varphi}}^{(e)} = 0 \tag{33}$$

Time discretization procedure is based on the forward Euler method. The procedure requires a time grid to be introduced

$$t^0, t^1, \ldots, t^{f-1}, t^f, \ldots, t^n \tag{34}$$

The time derivatives of T and φ in the range $\Delta t = t^{f+1} - t^f$ are approximated using the following difference schemes

$$t \in \left[t^{f-1}, t^f\right] : \dot{\mathbf{T}} = \frac{\mathbf{T}^f - \mathbf{T}^{f-1}}{\Delta t}, \dot{\boldsymbol{\varphi}} = \frac{\boldsymbol{\varphi}^f - \boldsymbol{\varphi}^{f-1}}{\Delta t} \tag{35}$$

These schemes are substituted into (32-33) and after elementary transformations and aggregation the following global FEM equations are obtained

$$\mathbf{T}^f = \Delta t \mathbf{M}_T^{-1} \left[\mathbf{B}_T + \left(\frac{1}{\Delta t} \mathbf{M}_T - \mathbf{K}_T \right) \mathbf{T}^{f-1} \right] \tag{36}$$

$$\boldsymbol{\varphi}^f = \Delta t \mathbf{M}_\phi^{-1} \left(\frac{1}{\Delta t} \mathbf{M}_\phi - \mathbf{A}_\phi \right) \boldsymbol{\varphi}^{f-1} \tag{37}$$

Dirichlet and Neumann boundary conditions are used to supplement (36). Assumed Neumann boundary condition here is the thermal insulation, q=0. Eq. (37) shows an initial problem, thus only initial condition is introduced, for example the position of the front at time t =0 [s].

Very important part of the presented model is the proper introduction of the continuity conditions (9-10). These conditions governs the velocity of the solidification interface. The main role plays here a narrow band of finite elements laying on the solidification interface as it is shown in Fig. 3. "Zone 0" is consisted of the elements cut by Γ_{LS} that is a discontinuity from the mathematical point of view. In the paper [23] an approach using discontinuous shape functions was proposed. In this work Γ_{LS} is diffused in the "zone 0" to avoid the difficulties associated with the discontinuity. Every node belonging to that region has melting temperature T_M, which is introduced to (36) in the form of Dirichlet boundary condition. "Zone 1" contains elements from the solid and liquid sides of Γ_{LS}. Temperature taken from the nodes laying on the solid and liquid sides of Γ_{LS} are used to calculate the heat fluxes on the interface. Then the velocity of Γ_{LS} is calculated according to (10).

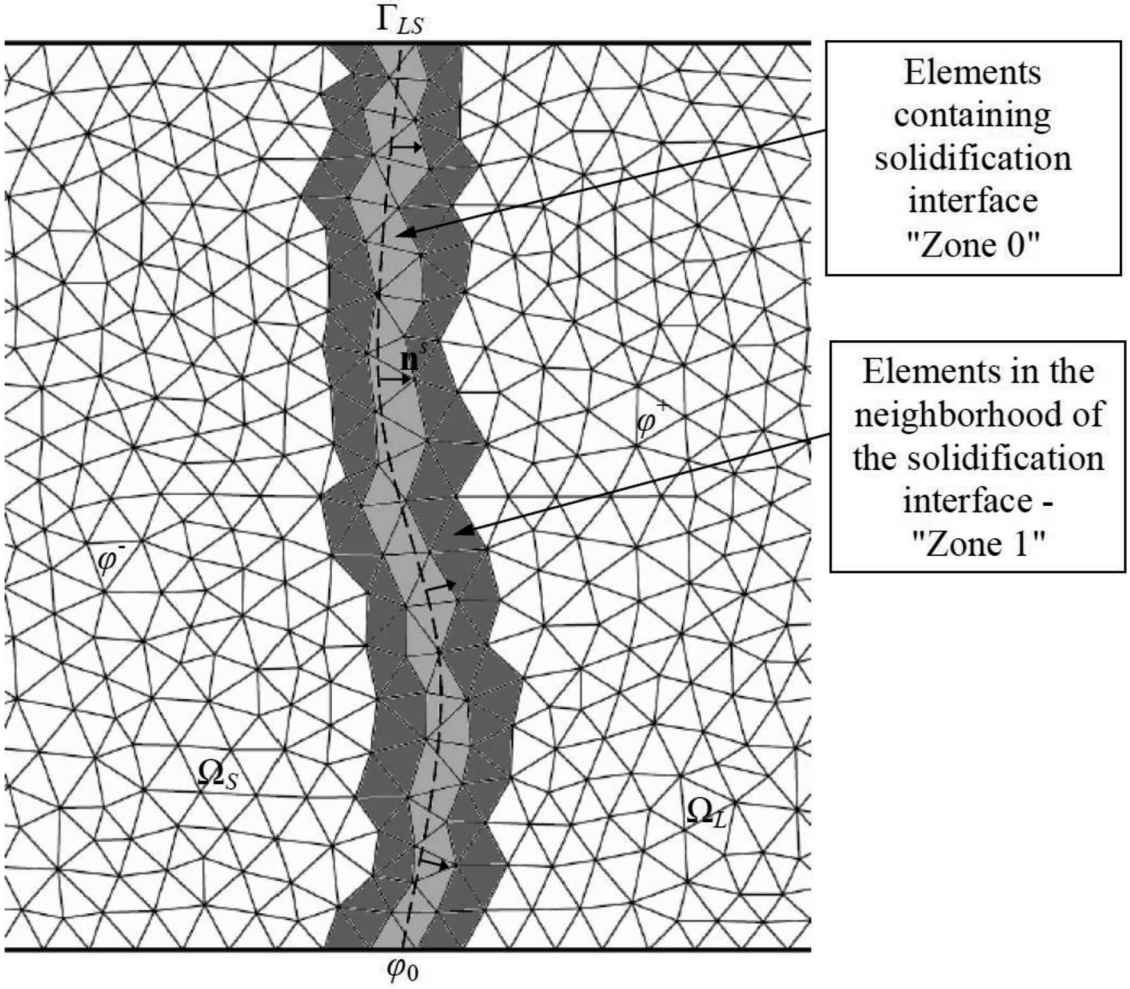

Fig. 3. Γ_{LS} surrounded by a narrow band of finite elements

In Fig. 4 the closest neighborhood of the solidifying element is shown. Light gray triangle has the temperature T_M because the melting point is set to all three nodes. Adjacent elements are dark grey. Five of them are used to calculate heat flux on the liquid side of Γ_{LS}. Heat fluxes in the directions x and y in each of these elements are calculated with the use of derivatives of shape functions and nodal temperatures

$$q_x^{(e_1)} = \lambda^{(e_1)} \sum_{i=1}^{3} \frac{\partial N_i}{\partial x} T_i, \quad q_y^{(e_1)} = \lambda^{(e_1)} \sum_{i=1}^{3} \frac{\partial N_i}{\partial y} T_i \tag{38}$$

Then the average fluxes are calculated using following formulas

$$q_x^{(liquid)} = \frac{1}{n} \sum_{j=1}^{n} q_x^{(e_j)}, \quad q_y^{(liquid)} = \frac{1}{n} \sum_{j=1}^{n} q_y^{(e_j)} \tag{39}$$

where n is the number of liquid neighbors of solidifying element.

Analogously heat flux in the solid is calculated using temperature taken from three elements lying on the solidified side of Γ_{LS}. This approach allows to calculate the average speed of Γ_{LS} in the solidifying element. Velocity of the front in the other elements are calculated in the same way.

The last problem that needs discussion is the reinitialization of the signed distance function φ [24, 25]. The evolution of (2) often distorts φ in a sense that its slope is too flat or too steep around Γ_{LS}. In such cases, a small perturbation of the level function may result in a big change of interface location, and the level function may lose enough regularity near the interface. Thus is very important to correct the values of φ to meet the following condition

$$|\nabla \phi| = 1 \tag{40}$$

Idea of the proposed method of reinitialization is shown in Fig. 4. It involves the introduction of the control points on the section of Γ_{LS} in the particular triangular element. Then the distances between them and the nodes n_1-n_{12} lying in the neighborhood are calculated and the smallest value is remembered. The operation is repeated for the whole front. The method is simple and effective.

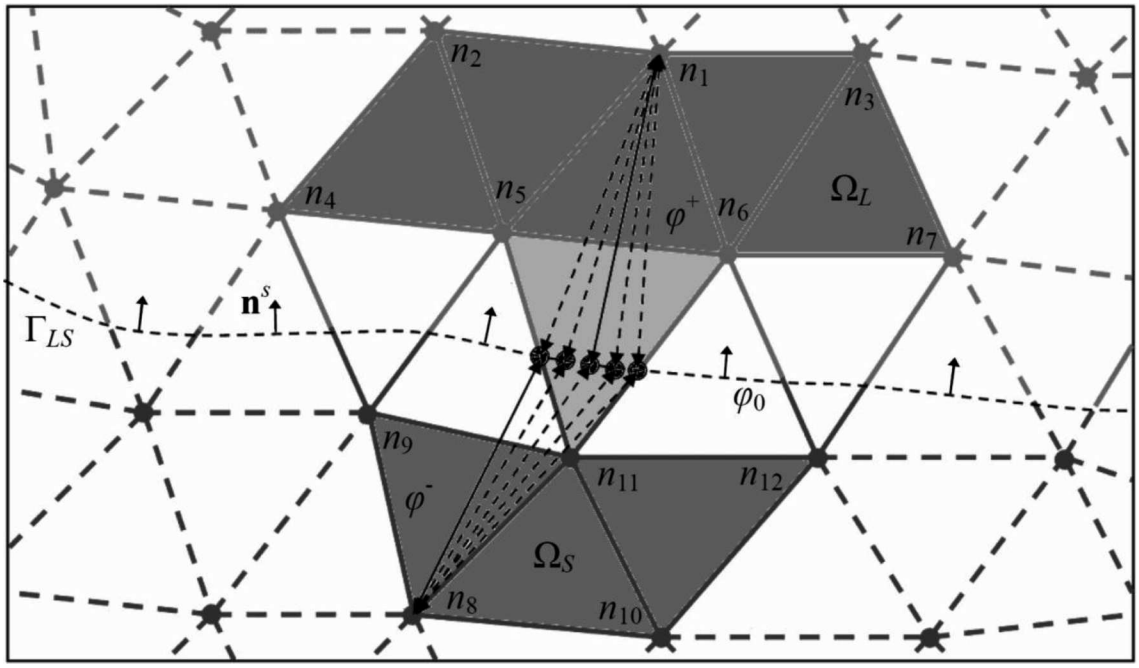

Fig. 4. Neighborhood of the element cut by Γ_{LS}

4. Examples of calculation

One of the major purposes of the calculation was to show the effectiveness and robustness of described numerical method in modeling of the solidification process of pure copper. The effects of applied method of front tracking were emphasized as well as reinitialization of level set function φ. Calculations were carried out in the complex planar geometry. Shape of the considered region was shown in Fig. 5 as well as initial and boundary conditions. Finite element mesh was composed of 328220 triangles with 164111 nodes. At time t=0 [s] the temperature of the entire region was uniform and equal to 1500 [K]. On the upper boundary the thermal insulation was employed. On the side boundaries Dirichlet boundary conditions were used with T_b=300 [K] as well as at the bottom, where the boundary temperature was equal to 600 [K].

Two numerical simulations were performed, the first using constant material properties (Table 1) and the second, which uses the temperature dependent properties (Table 2). The purpose of such approach was to show the differences between the results obtained from the calculations carried out with different thermophysical properties of copper. For the first calculation time step was equal to 2e-4 [s] while it was two times shorter for the second one. Shorter time step in the latter case was needed because of the temperature dependent material properties employed in the model.

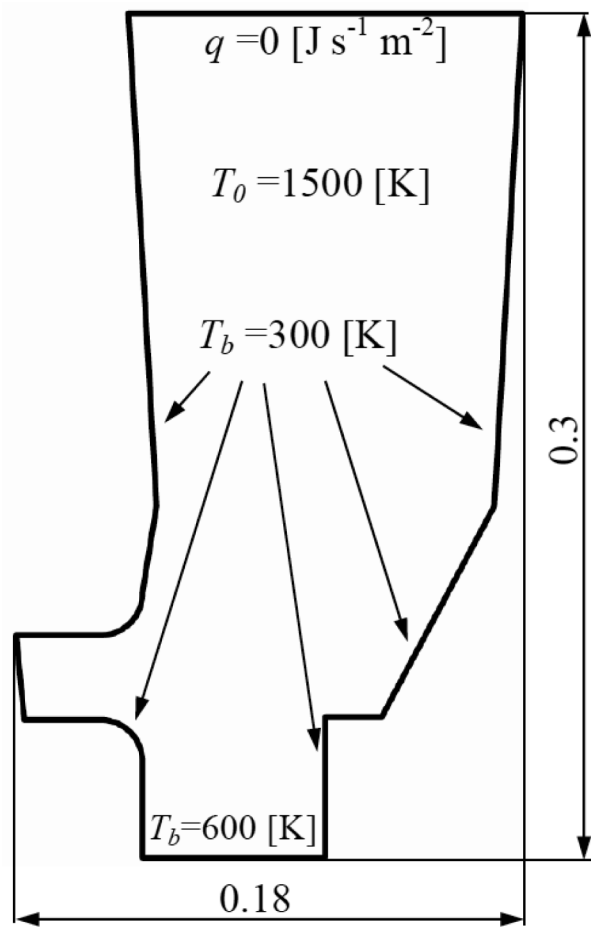

Fig. 5. Dimensions of the casting (in meters), boundary and initial conditions

TABLE 1
Material properties of pure copper independent of temperature [26]

Material property	Solid	Liquid
ρ [kg m^{-3}]	8920.0	8300.0
λ [J s^{-1} m^{-1} K^{-1}]	330.0	250.0
c [J kg^{-1} K^{-1}]	420.0	544.0
L [J kg^{-1}]	204000.0	
T_M [K]	1357.0	

The results included temporary distributions of the temperature as well as the positions and velocities of the solidification front. Temperature distributions at t=1 and t=15 [s] are shown in Fig. 6. Location of the melting point isotherm T_M=1357 [K] is marked by the dashed curve. Steep temperature gradient appearing on the solid side of the front is clearly noticeable as well as a much more flatter on the liquid one. Differences between the gradients were most pronounced at the very early stage of the process (Fig. 6a).

TABLE 2
Material properties of pure copper dependent on temperature [27-30]

T [K]	ρ [kg m^{-3}]	λ [J s^{-1} m^{-1} K^{-1}]	c [J kg^{-1} K^{-1}]
300.0	8933.0	401.0	385.0
400.0		393.0	398.44
500.0		386.5	408.0
600.0		379.0	417.0
700.0		372.8	425.0
800.0		366.0	432.0
900.0		359.11	441.0
1000.0		352.0	451.0
1100.0		345.41	464.0
1200.0		339.0	480.0
1300.0		331.71	506.0
1357.0	7998.0	160.0	495.0
1400.0	7962.0	162.0	
1450.0	7921.0	164.0	
1500.0	7881.0	166.0	

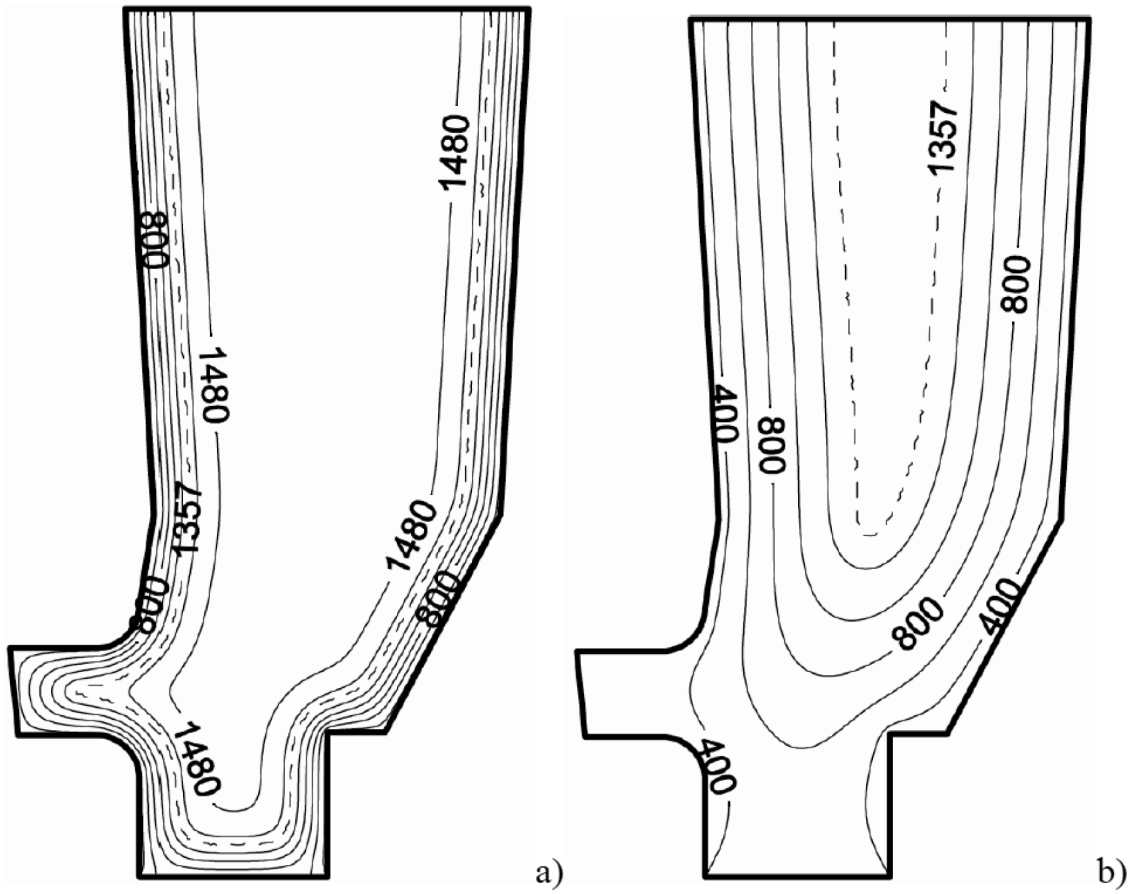

Fig. 6. Distribution of the temperature at a) t =1 [s], b) t =15 [s] (T_M is marked with dashed curve)

Temporary positions of the solidification interface obtained from the both cases of simulation are shown in Fig. 7. The comparison was done at selected moments t=1, t=5, t=10 and t=20 [s]. It shows that the differences between locations of the front at the early stage of the processes were negligible. They were getting more noticeable before the end of the solidification but in fact they were not significant comparing to the dimensions of the whole region.

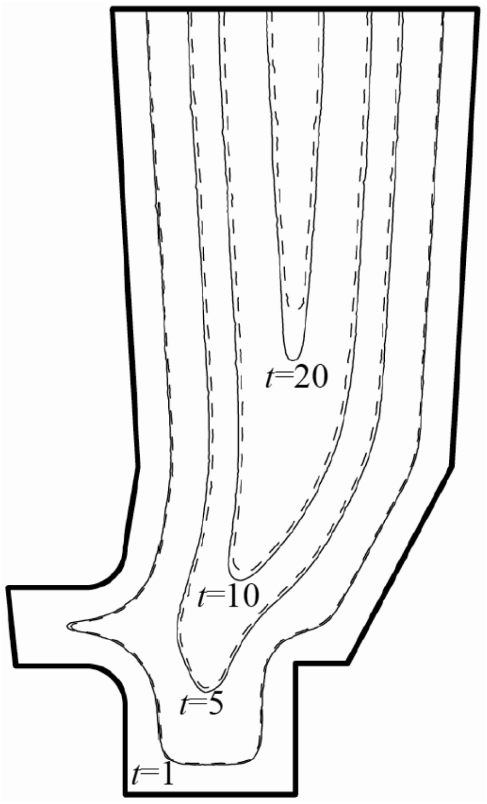

Fig. 7. Evolution of the solidification interface

The speed of the solidification front was calculated at each time step with the use of (10) in the nodes belonging to the narrow band of elements near the interface. Velocity vectors were directed normal to the interface as in Fig. 8. The front was moving from the cool boundaries to the centre of the casting keeping a direction perpendicular to the upper boundary.

The velocity of the solidification interface was decreasing rapidly according to time. The maximum velocity was at the start of the process due to the very steep temperature gradient in the solid layer near the cool boundaries (Fig. 9). At t=0.1 [s] the front was moving with the speed of 0.035 [m s^{-1}] and after several seconds its velocity decreased about ten times. One can observe that velocity of the sharp front during solidification of pure metal tends to a certain value. This value was in this case approximately equal to 0.003 [m s^{-1}].

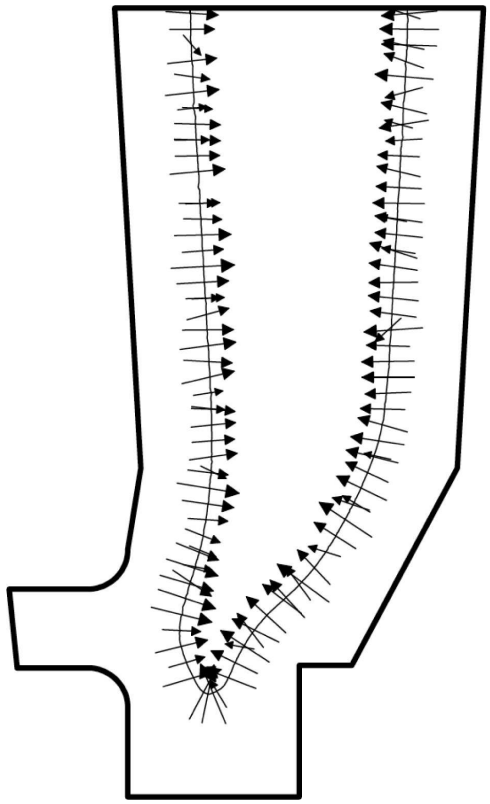

Fig. 8. Velocity vectors at the solidification front

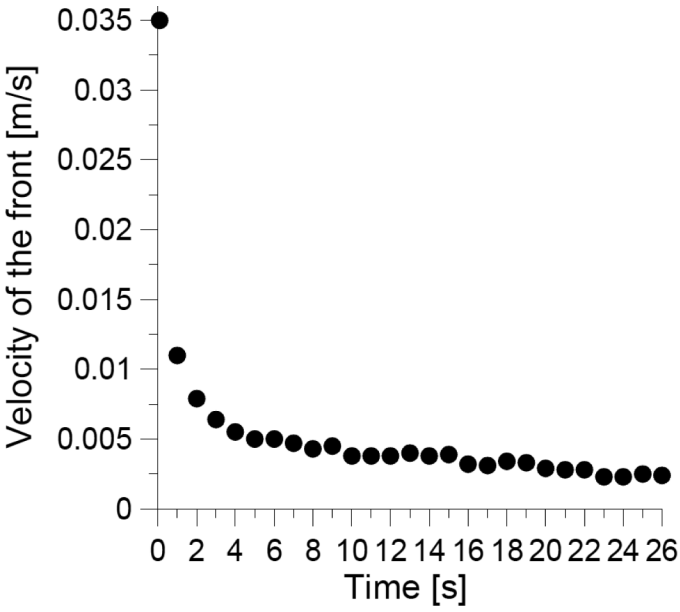

Fig. 9. Change of the maximum velocity of the front

The process ended after 26.4 [s] in the first case of computations and after 24.8 [s] in the second one. This shows that the differences between material properties had a very subtle impact on the duration of the solidification process.

5. Conclusions

Described mathematical and numerical models of solidification process of pure copper shows the possibility of introducing the continuity conditions at the sharp solidification front in the diffused form. The presented front tracking technique, based on the LSM proves its usefulness and robustness in solving the problems with moving internal boundaries. The formulation, based on the FEM was the basis for creation an in-home computer program. This is the solid beginning for further analysis of solidification process taking into account such phenomena as natural convection of the liquid phase or solute distribution.

REFERENCES

[1] B. Chalmers, Principles of solidification, Wiley, New York, 1964.

[2] K. Fisher, Fundamentals of solidification, fourth ed, Trans Tech Publications Ltd, Switzerland, 45-55 (1998).

[3] S. Chakraborty, P. Dutta, The effect of solutal undercooling on double-diffusive convection and macrosegregation during binary alloy solidification: a numerical investigation, International Journal for Numerical Methods in Fluids **38**, 895-917 (2002).

[4] S. Chakraborty, P. Dutta, Three-dimensional double-diffusive convection and macrosegregation during non-equilibrium solidification of binary mixtures, International Journal of Heat and Mass Transfer **46**, 2115-2134 (2003).

[5] T. Telejko, Z. Malinowski, M. Rywotycki, Analysis of heat transfer and fluid flow in continuous steel casting, Archives of Metallurgy and Materials **54**, 3, 837-844 (2009).

[6] L. Sowa, Numerical analysis of solid phase growing in a continuous steel caster, ZAMM **76**, 491-492 (1996).

[7] L. Sowa, A. Bokota, Numerical model of thermal and flow phenomena the process growing of the CC slab, Archives of Metallurgy and Materials **56**, 2, 359-366 (2011).

[8] W. Piekarska, M. Kubiak, A. Bokota, Numerical simulation of thermal phenomena and phase transformations in laser-arc hybrid welded joints, Archives of Metallurgy and Materials **56**, 2, 409-421 (2011).

[9] W. Piekarska, M. Kubiak, Three-dimensional model for numerical analysis of thermal phenomena in laser-arc hybrid welding process, International Journal of Heat and Mass Transfer **54**, 23-24, 4966-4974 (2011).

[10] A. Burbelko, J. Falkus, W. Kapturkiewicz, K. Sołek, P. Drożdż, M. Wróbel, Modeling of the grain structure formation in the steel continuous ingot by CAFE method, Archives of Metallurgy and Materials **57**, 1, 379-384 (2012).

[11] D. Gurgul, A. Burbelko, Simulation of austenite and graphite growth in ductile iron by means of cellular automata, Archives of Metallurgy and Materials **55**, 1, 53-60 (2010).

[12] W.J. Boettinger, J.A. Warren, C. Beckermann, A. Karma, Phase-field simulation of solidification, Annual Review of Materials Research **32**, 163-194 (2002).

[13] A. Karma, W.J. Rappel, Quantitative phase-field modelling of dendritic growth in two and three dimensions, Physical Review E **57**, 4323-4349 (1998).

[14] D.M. Anderson, G.B. McFadden, A.A. Wheeler, A phase-field model of solidification with convection, Physica D **135**, 175-194 (2000).

[15] S. Chen, B. Merriman, S. Osher, P. Smereka, A simple level set method for solving Stefan problems, Journal of Computational Physics **135**, 8-29 (1997).

[16] J. Chessa, P. Smolinski, T. Belytschko, The extended finite element method (XFEM) for solidification problems, International Journal for Numerical Methods in Engineering **53**, 1959-1977 (2002).

[17] G. Bell, A refinement of the heat balance integral method applied to a melting problem, International Journal of Heat and Mass Transfer **21**, 1357-1362 (1986).

[18] G. Comini, S.D. Guidice, R.W. Lewis, O.C. Zienkiewicz, Finite element solution on non-linear heat conduction problems with special reference to phase change, International Journal of Numerical Methods in Engineering **8**, 613-624 (1974).

[19] D. Rolph III, K.J. Bathe, An efficient algorithm for analysis of nonlinear heat transfer with phase change, International Journal of Numerical Methods in Engineering **18**, 119-134 (1982).

[20] D. Adalsteinsson, J.A. Sethian, A fast level set method for propagating interfaces, Journal of Computational Physics **118**, 269-277 (1995).

[21] T. Barth, J. Sethian, Numerical schemes for the hamilton-jacobi and level set equations on triangulated domains, Journal of Computational Physics **145**, 1-40 (1998).

[22] S. Osher, J.A. Sethian, Fronts propagating with curvature-dependent speed: Algorithms based on the Hamilton-Jacobi formulation, Journal of Computational Physics **79**, 12-49 (1988).

[23] T. Skrzypczak, E. Węgrzyn-Skrzypczak, Mathematical and numerical model of solidification process of pure metals, International Journal of Heat and Mass Transfer **55**, 4276-4284 (2012).

[24] D. Peng, B. Merriman, S. Osher, H. Zhao, A PDE-based fast local level set method, Journal of Computational Physics **155**, 410-438 (1999).

[25] M. Sussman, E. Fatemi, An efficient interface preserving level set re-distancing algorithm and its applications to interfacial incompressible fluid flow, Journal of Scientific Computing **20**, 1165-1191 (1999).

[26] B. Mochnacki, J.S. Suchy, Modelowanie i symulacja krzepnięcia odlewów, Wydawnictwo Naukowe PWN, Warszawa, 208, 1993.
[27] M.J. Assael, A.E. Kalyva, K.D. Antoniadis, Reference data for the density and viscosity of liquid copper and liquid tin, Journal of Physical and Chemical Reference Data **39**, 3, 033105-033105-8 (2010).
[28] G.K. White, S.J. Collocott, Heat capacity of reference materials: Cu and W, Journal of Physical and Chemical Reference Data **13**, 4, 1251-1257 (1984).
[29] T.J. Miller, S.J. Zinkle, B.A. Chin, Strength and fatigue of dispersion-strengthened Copper, Journal of Nuclear Materials **179-181**, 263-266 (1991).
[30] F.P. Incropera, D.P. Dewitt, Fundamentals of heat and mass transfer, 2nd ed., Wiley, New York, 1995.

Received: 10 May 2012.